01 Nov 2017

Drained Elastoplastic Solution For Cylindrical Cavity Expansion In K0-consolidated Anisotropic Soil

Jingpei Li

Weibing Gong
Missouri University of Science and Technology, weibing.gong@mst.edu

Lin Li

Fang Liu

Recommended Citation

J. Li et al., "Drained Elastoplastic Solution For Cylindrical Cavity Expansion In K0-consolidated Anisotropic Soil," *Journal of Engineering Mechanics*, vol. 143, no. 11, article no. 04017133, American Society of Civil Engineers, Nov 2017.
The definitive version is available at https://doi.org/10.1061/(ASCE)EM.1943-7889.0001357

Drained Elastoplastic Solution for Cylindrical Cavity Expansion in K_0-Consolidated Anisotropic Soil

Jingpei Li[1]; Weibing Gong[2]; Lin Li[3]; and Fang Liu[4]

Abstract: This paper presents a semianalytical solution for drained expansion of a cylindrical cavity in K_0-consolidated clay. The solution is derived based on the K_0-based anisotropic modified Cam-clay model (K_0-AMCC), which can properly consider the initial stress anisotropy and the initial stress-induced anisotropy of natural soils. Parametric studies are carried out to investigate the effects of different overconsolidation ratios on the growth of plastic zone and cavity pressure, the distributions of the stress components and the specific volume around the cavity, and the effective stress path. The results are compared with the published solution based on the modified Cam-clay model to study the effects of the initial stress anisotropy and the initial stress-induced anisotropy on the cylindrical cavity expansion. The present solution provides a more realistic interpretation for practical geotechnical engineering problems such as pressuremeter tests and cone penetration tests. **DOI: 10.1061/(ASCE)EM.1943-7889.0001357.** © *2017 American Society of Civil Engineers.*

Author keywords: Drained expansion; K_0-based anisotropic modified Cam-clay model (K_0-AMCC); Initial stress anisotropy; Initial stress-induced anisotropy.

Introduction

The cylindrical cavity expansion theory theoretically analyzes the stress and displacement fields around cylindrical cavities. This theory was initially explored by Lamé (1852) in a linear elastic medium, and extended to many engineering applications associated with more complex materials. The cylindrical cavity expansion theory has become a fundamental tool for modeling complex geotechnical problems in theoretical geomechanics. Such examples include the interpretation of pressuremeter tests and cone penetration tests (Collins and Stimpson 1994; Yu et al. 1996; Chang et al. 2001; Falagush et al. 2015; Mo et al. 2017), installation of driven piles (Randolph et al. 1979; Mabsout et al. 1999; Guo 2000; Randolph 2003; Li et al. 2017), and underground tunneling (Yu and Rowe 1999; Yu 2000; Vrakas and Anagnostou 2015). Moreover, this theory has been adopted to estimate the effects of tunnel construction on end-bearing piles (Marshall 2012).

To solve the expansion problems of cylindrical cavity in soils, a constitutive relationship is required to describe the stress-strain behavior of soils during expansion. Unlike concrete and steel, soils are natural construction materials with mechanical properties that are more difficult to determine because of the complex sedimentary environment and consolidation history. Initially, the Tresca and Mohr-Coulomb failure criteria were widely used to determine the stress-strain behavior of soils. However, they introduced too many idealizations and simplifications that overlook real soil behavior, so the Cam-clay critical state models (Roscoe et al. 1963; Schofield and Wroth 1968; Wood 1990) were developed. After approximately 100 years of development, there are many soil constitutive relationships at present. Different soil constitutive relationships lead to various solutions for cylindrical cavity expansion. The Tresca and Mohr-Coulomb failure criteria, two popular soil constitutive relationships, are widely used to derive analytical or semianalytical solutions for cylindrical cavity expansion. Hill (1950) used the Tresca plasticity criterion to present a comprehensive analysis of the stresses and displacements for the expansion of a cylindrical cavity. Vesic (1972) proposed a general solution for the expansion of spherical and cylindrical cavities in a Mohr-Coulomb soil by considering volume change in the plastic region. Carter et al. (1986) presented closed-form solutions for the expansion of cylindrical and spherical cavities in a Mohr-Coulomb soil to obtain the complete pressure-expansion relationship. Frikha and Bouassida (2013) determined the limit pressure of a laterally expanded cylindrical cavity by developing the Mohr-Coulomb strength criterion with a variable potential flow. Zhou et al. (2014) analytically explored an undrained cylindrical cavity expansion under anisotropic initial stress with the Tresca failure criterion. Zhou et al. (2016) semianalytically investigated an undrained cylindrical cavity expansion under biaxial in situ stress field based on the Tresca failure criterion with the associated flow rule. Although the Tresca and Mohr-Coulomb failure criteria can capture, to some extent, major behaviors of soils during cavity expansion, they are incapable of modeling the strain-hardening or strain-softening behaviors of soils.

Alternatively, the Cam-clay critical state models have been used to further develop the cylindrical cavity expansion theory. These models pay more attention to volumetric changes in addition to variation of effective stress in soil mass during shearing. For instance, Carter et al. (1979) derived numerical solutions for cylindrical cavity expansion based on the Cam-clay hardening critical state model to study the stress and pore pressure changes in clay. Collins and Yu (1996) described the soil behavior based on various critical state models during cavity expansion, and used the solutions to predict the excess pore pressures during pile installation

[1]Professor, Dept. of Geotechnical Engineering, Tongji Univ., Shanghai 200092, China (corresponding author). E-mail: lijp2773@163.com

[2]Master's Degree Candidate, Dept. of Geotechnical Engineering, Tongji Univ., Shanghai 200092, China. E-mail: weibingthomas@163.com

[3]Ph.D. Student, Dept. of Geotechnical Engineering, Tongji Univ., Shanghai 200092, China. E-mail: lilin_sanmao@163.com

[4]Associate Professor, State Key Laboratory of Disaster Reduction in Civil Engineering, Tongji Univ., Shanghai 200092, China; Associate Professor, Dept. of Geotechnical Engineering, Tongji Univ., Shanghai 200092, China. E-mail: liufang@tongji.edu.cn

Note. This manuscript was submitted on July 28, 2016; approved on May 24, 2017; published online on September 11, 2017. Discussion period open until February 11, 2018; separate discussions must be submitted for individual papers. This paper is part of the ***Journal of Engineering Mechanics***, © ASCE, ISSN 0733-9399.

in overconsolidated clays. Cao et al. (2001) presented both exact and approximate closed-form solutions for undrained cavity expansion using the modified Cam-clay (MCC) model by assuming small strain in the elastic zone and large strain in the plastic zone. Chen and Abousleiman (2012) also established a theoretical framework for the undrained cylindrical cavity expansion based on the MCC model, but the deviator and mean effective stresses were exact and the shear modulus was a variable in proportion to the mean effective stress. Li et al. (2016a) derived a semianalytical solution to improve the undrained solution of Chen and Abousleiman (2012), which can consider the anisotropy of natural clays during cavity expansion. Li et al. (2016b) used the spatially mobilized method to consider the three-dimensional strength of soils when analyzing the undrained cylindrical cavity expansion. Mo and Yu (2017) proposed an analytical solution for undrained expansion of spherical and cylindrical cavities with a unified state parameter model for clay and sand, which is actually an improved Cam-clay critical state model. However, the aforementioned studies have not been extended to drained conditions, which are commonly seen in soils with large permeability and subjected to slow loading process. Drained conditions will introduce further complexity to the derivation because the soil volume is variable and the specific volume needs to be determined as one of the unknowns. Moreover, most of these studies neglect the effect of the in situ anisotropic stresses and the initial stress-induced anisotropy. Chen and Abousleiman (2013) attempted to develop an exact solution for drained cylindrical cavity expansion by introducing an auxiliary variable; however, they only considered the effect of the in situ anisotropic stresses and neglected the effect of the initial stress-induced anisotropy on the cavity expansion. Natural soils usually consolidate in the K_0 condition (where K_0 denotes the coefficient of earth pressure at rest) and thus exhibit initial stress anisotropy and initial stress-induced anisotropic properties. However, to the best of authors' knowledge, the solutions for drained cylindrical cavity expansion in a K_0-consolidated soil are still not available at present.

This paper models the soil behavior during cylindrical cavity expansion using the K_0-based anisotropic modified Cam-clay (K_0-AMCC) model, which is a highly sophisticated model that can incorporate the initial stress anisotropy and the initial stress-induced anisotropy of natural soils. An auxiliary variable defined as the ratio of the radial displacement of a soil element to the current place of the soil element (Chen and Abousleiman 2013) is introduced to make the drained cylindrical cavity expansion problem as an initial value problem in terms of Lagrangian form. The solutions are compared with the results of the published drained solutions built on the MCC model. The stress state of a soil element during the expansion of cylindrical cavity is illustrated by effective stress path (ESP). The three-dimensional property of the ESPs is reflected by plotting them in the p'–q and deviator planes.

Problem Definition

Fig. 1 schematically shows the expansion of a cylindrical cavity in the K_0-consolidated soil, which is subjected to an initial horizontal stress, σ'_{h0}, and an initial vertical stress, σ'_{z0}. The cavity radius expands from the initial radius, a_0, to the current radius, a, due to the increase of the internal cavity pressure. Correspondingly, a radial displacement of the soil element, u, is generated and equal to the difference between the new radial position, r, and the initial radial position, r_0 (i.e., $u = r - r_0$). As the internal cavity pressure continuously increases, the soil yields and the plastic zone expands. The notation r_y denotes the distance of the elastic-plastic boundary from the cavity center. The assumptions for the present analytical

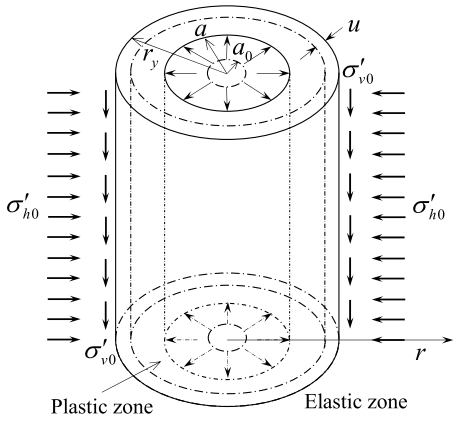

Fig. 1. Drained cylindrical cavity expansion in K_0-consolidated soil

framework of the drained cylindrical cavity expansion are as follows:

1. The K_0-consolidated soil is homogeneous and follows Hooke's law in the elastic zone. The behavior of the yielded soil is described by the K_0-AMCC model and large deformation theory.
2. The expansion of the cylindrical cavity is under the plane strain condition. Conventionally, the compressive stress and strain components are assumed to be positive.

In both plastic and elastic zones, the equilibrium equation of a soil element can be expressed in terms of the cylindrical polar coordinates as (Carter et al. 1979)

$$\frac{d\sigma'_r}{dr} + \frac{\sigma'_r - \sigma'_\theta}{r} = 0 \tag{1}$$

where σ'_r = radial stress; and σ'_θ = circumferential stress. The pore pressure remains constant under the drained condition and needs no consideration in the analysis. Hence the term stress in this study should be interpreted as effective stress.

Anisotropic Solutions for Cylindrical Cavity Expansion

Elastic Analysis

By Hooke's law and small strain theory, the solutions for stress components in the elastic zone and the radial displacement of the soil element can be obtained as (Cao et al. 2001)

$$\sigma'_r = \sigma'_h + (\sigma'_y - \sigma'_h)\left(\frac{r_y}{r}\right)^2 \tag{2}$$

$$\sigma'_\theta = \sigma'_h - (\sigma'_y - \sigma'_h)\left(\frac{r_y}{r}\right)^2 \tag{3}$$

$$\sigma'_z = \sigma'_v \tag{4}$$

$$u = \frac{\sigma'_y - \sigma'_h}{2G_0}\frac{r_y^2}{r} \tag{5}$$

where σ'_y = stress at the elastic-plastic boundary; and G_0 = initial shear modulus, defined as (Wood 1990)

$$G_0 = \frac{3(1-2v')v_0 p'_0}{2(1+v')\kappa} \tag{6}$$

where v' = Poisson's ratio; v_0 = initial specific volume; κ = slope of the unloading line in the $v - \ln p'$ plane; and p'_0 = initial mean stress.

Elastoplastic Analysis

In the K_0-AMCC model, two parameters (i.e., the relative stress ratio, η^*, and the relative stress ratio at the critical state, M^*) are introduced to consider the initial stress anisotropy and the initial stress-induced anisotropy of natural soils. Considering the strain hardening rule, the yielding function of K_0-AMCC model is (Matsuoka and Sun 2006; Yao et al. 2009)

$$f = \frac{\lambda - \kappa}{1 + e_0} \ln \frac{p'}{p'_0} + \frac{\lambda - \kappa}{1 + e_0} \ln \left[1 + \left(\frac{\eta^*}{M^*} \right)^2 \right] - \varepsilon_v^p \tag{7}$$

where λ = slope of the loading line in the $v - \ln p'$ plane; e_0 = initial void ratio; p' = mean stress; and ε_v^p = plastic volume strain, used as the hardening parameter in the model. The relative stress ratio, η^*, and the relative stress ratio at the critical state, M^*, are defined as

$$\eta^* = \sqrt{\frac{3}{2}(\eta_{ij} - \eta_{ij0})(\eta_{ij} - \eta_{ij0})} \tag{8}$$

$$M^* = \sqrt{M^2 - \eta_0^2} \tag{9}$$

where

$$\eta_{ij} = \frac{\sigma'_{ij} - p'\delta_{ij}}{p'} \tag{10}$$

$$\eta_{ij0} = \frac{\sigma'_{ij0} - p'_0\delta_{ij}}{p'_0} \tag{11}$$

$$\eta_0 = \left| \frac{3(1 - K_0)}{2K_0 + 1} \right| \tag{12}$$

where $\eta(= q/p')$ = stress ratio; δ_{ij} = Kronecker's delta; and M = slope of the critical line.

The K_0-AMCC model adopts the associated flow rule in the derivation process because the K_0-AMCC model is based in the framework of the Cam-clay model, and obeying the associated flow rule is one of the basic assumptions of the Cam-clay model. Thus the plastic strain increment is normal to the yield function and leads to

$$d\varepsilon_{ij}^p = \Lambda \frac{\partial f}{\partial \sigma'_{ij}} \tag{13}$$

where Λ = scalar, given as

$$\Lambda = -\frac{(\partial f/\partial p')dp' + (\partial f/\partial \eta^*)d\eta^*}{(\partial f/\partial \varepsilon_v^p)(\partial f/\partial \sigma'_{ij})} \tag{14}$$

Differentiating Eq. (7) with respect to p', η^*, ε_v^p and σ'_{ij}, respectively, yields

$$\frac{\partial f}{\partial p'} = \frac{\lambda - \kappa}{1 + e_0} \frac{1}{p'} \tag{15}$$

$$\frac{\partial f}{\partial \eta^*} = \frac{\lambda - \kappa}{1 + e_0} \frac{2\eta^*}{M^{*2} + \eta^{*2}} \tag{16}$$

$$\frac{\partial f}{\partial \varepsilon_v^p} = -1 \tag{17}$$

$$\frac{\partial f}{\partial \sigma'_{ij}} = \frac{\partial f}{\partial p'} \frac{\partial p'}{\partial \sigma'_{ij}} + \frac{\partial f}{\partial \eta^*} \frac{\partial \eta^*}{\partial \sigma'_{ij}} \tag{18}$$

where

$$\frac{\partial p'}{\partial \sigma'_{ij}} = \frac{\delta_{ij}}{3} \tag{19}$$

$$\frac{\partial \eta^*}{\partial \sigma'_{ij}} = \frac{1}{2\eta^* p'} [3(\eta_{ij} - \eta_{ij0}) - \eta_{kl}(\eta_{kl} - \eta_{kl0})\delta_{ij}] \tag{20}$$

Substituting Eqs. (19) and (20) into Eq. (18) leads to

$$\frac{\partial f}{\partial \sigma'_{ij}} = \frac{\lambda - \kappa}{1 + e_0} \frac{1}{p'} \left[\frac{\delta_{ij}}{3} + \frac{3(\eta_{ij} - \eta_{ij0}) - \eta_{kl}(\eta_{kl} - \eta_{kl0})\delta_{ij}}{M^{*2} + \eta^{*2}} \right] \tag{21}$$

From Eq. (20), the derivative of η^* can be obtained as

$$d\eta^* = \frac{\partial \eta^*}{\partial \sigma'_{ij}} d\sigma'_{ij} = \frac{1}{2\eta^* p'} [3(\eta_{ij} - \eta_{ij0}) - \eta_{kl}(\eta_{kl} - \eta_{kl0})\delta_{ij}] d\sigma'_{ij} \tag{22}$$

The plastic strain increment, $d\varepsilon_{ij}^p$, then can be determined as

$$\begin{aligned} d\varepsilon_{ij}^p = {} & \frac{\lambda - \kappa}{1 + e_0} \frac{1}{p'} \frac{M^{*2} + \eta^{*2}}{M^{*2} + \eta^{*2} - 3\eta_{kl}(\eta_{kl} - \eta_{kl0})} \\ & \times \left[\frac{\delta_{ij}}{3} + \frac{3(\eta_{ij} - \eta_{ij0}) - \eta_{kl}(\eta_{kl} - \eta_{kl0})\delta_{ij}}{M^{*2} + \eta^{*2}} \right] \\ & \times \left[\frac{\delta_{ij}}{3} + \frac{3(\eta_{ij} - \eta_{ij0}) - \eta_{kl}(\eta_{kl} - \eta_{kl0})\delta_{ij}}{M^{*2} + \eta^{*2}} \right] d\sigma_{ij} \end{aligned} \tag{23}$$

Eq. (23) can be rewritten in matrix form as

$$\begin{Bmatrix} d\varepsilon_r^p \\ d\varepsilon_\theta^p \\ d\varepsilon_z^p \end{Bmatrix} = \psi \begin{bmatrix} c_r^2 & c_r c_\theta & c_r c_z \\ c_r c_\theta & c_\theta^2 & c_\theta c_z \\ c_r c_z & c_\theta c_z & c_z^2 \end{bmatrix} \begin{Bmatrix} d\sigma'_r \\ d\sigma'_\theta \\ d\sigma'_z \end{Bmatrix} \tag{24}$$

where

$$c_r = \frac{1}{3} + \frac{3(\eta_r - \eta_{r0}) - \eta_{kl}(\eta_{kl} - \eta_{kl0})}{M^{*2} + \eta^{*2}} \tag{25}$$

$$c_\theta = \frac{1}{3} + \frac{3(\eta_\theta - \eta_{\theta 0}) - \eta_{kl}(\eta_{kl} - \eta_{kl0})}{M^{*2} + \eta^{*2}} \tag{26}$$

$$c_z = \frac{1}{3} + \frac{3(\eta_z - \eta_{z0}) - \eta_{kl}(\eta_{kl} - \eta_{kl0})}{M^{*2} + \eta^{*2}} \tag{27}$$

$$\psi = \frac{\lambda - \kappa}{1 + e_0} \frac{1}{p'} \frac{M^{*2} + \eta^{*2}}{M^{*2} + \eta^{*2} - 3\eta_{kl}(\eta_{kl} - \eta_{kl0})} \tag{28}$$

When the soil enters the plastic state, the total strain increment, $d\varepsilon_{ij}$, is composed of the elastic strain increment, $d\varepsilon_{ij}^e$, and the plastic strain increment, $d\varepsilon_{ij}^p$, namely

$$d\varepsilon_{ij} = d\varepsilon_{ij}^e + d\varepsilon_{ij}^p \tag{29}$$

The elastic strain increment, $d\varepsilon_{ij}^{e}$, can be determined by Hooke's law as

$$de_{ij}^{e} = \frac{1+v'}{E} d\sigma'_{ij} - \frac{v'}{E} d\sigma'_{mm}\delta_{ij} \tag{30}$$

The constitutive equation can be obtained by substituting Eqs. (24) and (30) into Eq. (29) as

$$\begin{Bmatrix} d\varepsilon_r \\ d\varepsilon_\theta \\ d\varepsilon_z \end{Bmatrix} = \begin{bmatrix} \frac{1}{E}+\psi c_r^2 & -\frac{v'}{E}+\psi c_r c_\theta & -\frac{v'}{E}+\psi c_r c_z \\ -\frac{v'}{E}+\psi c_r c_\theta & \frac{1}{E}+\psi c_\theta^2 & -\frac{v'}{E}+\psi c_\theta c_z \\ -\frac{v'}{E}+\psi c_r c_z & -\frac{v'}{E}+\psi c_\theta c_z & \frac{1}{E}+\psi c_z^2 \end{bmatrix} \begin{Bmatrix} d\sigma'_r \\ d\sigma'_\theta \\ d\sigma'_z \end{Bmatrix} \tag{31}$$

The constitutive equations can be inversely expressed as

$$\begin{Bmatrix} d\sigma'_r \\ d\sigma'_\theta \\ d\sigma'_z \end{Bmatrix} = \frac{1}{\Omega} \begin{bmatrix} \xi_{11} & \xi_{12} & \xi_{13} \\ \xi_{21} & \xi_{22} & \xi_{23} \\ \xi_{31} & \xi_{32} & \xi_{31} \end{bmatrix} \begin{Bmatrix} d\varepsilon_r \\ d\varepsilon_\theta \\ d\varepsilon_z \end{Bmatrix} \tag{32}$$

where

$$\xi_{11} = \frac{1}{E^2}(Ec_\theta^2\psi + Ec_z^2\psi + 2Ev'c_\theta c_z\psi + 1 - v'^2) \tag{33}$$

$$\xi_{22} = \frac{1}{E^2}(Ec_r^2\psi + Ec_z^2\psi + 2Ev'c_r c_z\psi + 1 - v'^2) \tag{34}$$

$$\xi_{33} = \frac{1}{E^2}(Ec_r^2\psi + Ec_\theta^2\psi + 2Ev'c_\theta c_z\psi + 1 - v'^2) \tag{35}$$

$$\xi_{12} = \xi_{21} = \frac{1}{E^2}[v'(1+v' - Ec_\theta c_z\psi + Ec_z^2\psi) - Ec_r(c_\theta + v'c_z)\psi] \tag{36}$$

$$\xi_{13} = \xi_{31} = \frac{1}{E^2}[v'(1+v' - Ec_\theta c_z\psi + Ec_\theta^2\psi) - Ec_r(c_z + v'c_\theta)\psi] \tag{37}$$

$$\xi_{23} = \xi_{32} = \frac{1}{E^2}[v' + v'^2 + Ev'c_r^2\psi - Ev'c_r(c_\theta + c_r)\psi - Ec_\theta c_z\psi] \tag{38}$$

$$\begin{aligned}\Omega = -\frac{1+v'}{E^3}[&(-1+v'+2v'^2) + E(-1+v')c_r^2\psi \\ &+ E(-1+v')c_\theta^2\psi - 2Ev'c_\theta c_z\psi - Ec_z^2\psi + Ev'c_z^2\psi \\ &- 2Ev'c_r(c_\theta + c_z)\psi]\end{aligned} \tag{39}$$

Because the cylindrical cavity expansion is under the plane strain condition, the vertical strain increment, $d\varepsilon_z$, is 0. Thus the volumetric strain increment has the following relationship:

$$d\varepsilon_v = d\varepsilon_r + d\varepsilon_\theta \tag{40}$$

The volumetric strain increment can be defined as

$$d\varepsilon_v = -\frac{dv}{v} \tag{41}$$

where v = specific volume. Introducing Eqs. (40) and (41) into Eq. (32) yields

$$d\sigma'_r = \frac{1}{\Omega}\left[\xi_{11}\left(-\frac{dv}{v}\right) + (\xi_{12} - \xi_{11})d\varepsilon_\theta\right] \tag{42}$$

$$d\sigma'_\theta = \frac{1}{\Omega}\left[\xi_{21}\left(-\frac{dv}{v}\right) + (\xi_{22} - \xi_{21})d\varepsilon_\theta\right] \tag{43}$$

$$d\sigma'_z = \frac{1}{\Omega}\left[\xi_{31}\left(-\frac{dv}{v}\right) + (\xi_{32} - \xi_{31})d\varepsilon_\theta\right] \tag{44}$$

For the drained condition, the specific volume, v, does not remain constant (i.e., $dv \neq 0$) and needs to be determined during the cavity expansion. The variable specific volume indicates that the constitutive equations have four unknowns, whereas there are only three equations. Hence it is impossible to obtain the stress components directly based on the above differential equations. In order to overcome this barrier, an auxiliary variable is introduced to convert the Eulerian equilibrium equation [Eq. (1)] into the Lagrangian form, which is defined as (Chen and Abousleiman 2013)

$$\chi = \frac{u}{r} = \frac{r - r_0}{r} \tag{45}$$

The tangential strain increment in the logarithmic form can consider the large deformation in the plastic zone and is defined as (Chen and Abousleiman 2013)

$$d\varepsilon_\theta = -\frac{dr}{r} \tag{46}$$

Substitution of Eqs. (45) and (46) into Eqs. (42)–(44) yields the following:

$$\frac{d\sigma'_r}{d\chi} = \frac{1}{\Omega}\left(\frac{\xi_{11} - \xi_{12}}{1-\chi} - \frac{\xi_{11}g}{v}\right) \tag{47}$$

$$\frac{d\sigma'_\theta}{d\chi} = \frac{1}{\Omega}\left(\frac{\xi_{21} - \xi_{22}}{1-\chi} - \frac{\xi_{21}g}{v}\right) \tag{48}$$

$$\frac{d\sigma'_z}{d\chi} = \frac{1}{\Omega}\left(\frac{\xi_{31} - \xi_{32}}{1-\chi} - \frac{\xi_{31}g}{v}\right) \tag{49}$$

$$g = \frac{dv}{d\chi} \tag{50}$$

Although four equations have been obtained by introducing the auxiliary variable, χ, there are still five unknowns required to be determined, i.e., σ'_r, σ'_θ, σ'_z, χ, and g. Hence an additional equation should be provided to solve all the unknowns. The equilibrium equation of the soil element [i.e., Eq. (1)] is rewritten with respect to the auxiliary variable, χ, as

$$\frac{d\sigma'_r}{d\chi}\frac{d\chi}{dr} + \frac{\sigma'_r - \sigma'_\theta}{r} = 0 \tag{51}$$

Eliminating $d\sigma'_r/d\chi$ from Eqs. (47) and (51) and substituting Eq. (45) into Eq. (51) leads to

$$\frac{1}{\Omega}\left(\frac{\xi_{11} - \xi_{12}}{1-\chi} - \frac{\xi_{11}g}{v}\right)\left(\frac{du}{dr} - \chi\right) + (\sigma'_r - \sigma'_\theta) = 0 \tag{52}$$

Under the drained and plane strain conditions, the radial strain, ε_r, can be determined from

J. Eng. Mech., 2017, 143(11): 04017133

$$\varepsilon_r = \varepsilon_v - \varepsilon_\theta = -\ln\left(\frac{\upsilon}{\upsilon_0}\right) + \ln\left(\frac{r}{r_0}\right) = \ln\frac{\upsilon_0}{\upsilon(1-\chi)} \tag{53}$$

The natural radial strain can be defined and rearranged as

$$\varepsilon_r = -\ln\left(\frac{dr}{dr_0}\right) = -\ln\left(1 + \frac{du}{dr}\frac{dr}{dr_0}\right) = -\ln\left(1 + \frac{du}{dr}e^{-\varepsilon_r}\right) \tag{54}$$

Combining Eqs. (53) and (54) gives

$$\frac{du}{dr} = 1 - \frac{\upsilon_0}{\upsilon(1-\chi)} \tag{55}$$

Substituting Eq. (55) into Eq. (52) gives the expression of the function g as

$$g = \frac{d\upsilon}{d\chi} = \frac{\upsilon}{\xi_{11}}\left[\frac{\xi_{11}-\xi_{12}}{1-\chi} + \frac{\upsilon\Omega(1-\chi)(\sigma_r'-\sigma_\theta')}{\upsilon(1-\chi)^2-\upsilon_0}\right] \tag{56}$$

The function g is related to the stress components and the specific volume. In addition, the expressions of the stress components can be obtained by substituting Eq. (55) into Eqs. (47)–(49) as follows:

$$\frac{d\sigma_r'}{d\chi} = \frac{\upsilon\Omega(1-\chi)(\sigma_r'-\sigma_\theta')}{\upsilon(1-\chi)^2-\upsilon_0} \tag{57}$$

$$\frac{d\sigma_\theta'}{d\chi} = \frac{1}{\Omega}\left\{\frac{\xi_{21}-\xi_{22}}{1-\chi} - \frac{\xi_{21}}{\xi_{11}}\left[\frac{\xi_{11}-\xi_{12}}{1-\chi} + \frac{\upsilon\Omega(1-\chi)(\sigma_r'-\sigma_\theta')}{\upsilon(1-\chi)^2-\upsilon_0}\right]\right\} \tag{58}$$

$$\frac{d\sigma_z'}{d\chi} = \frac{1}{\Omega}\left\{\frac{\xi_{31}-\xi_{32}}{1-\chi} - \frac{\xi_{31}}{\xi_{11}}\left[\frac{\xi_{11}-\xi_{12}}{1-\chi} + \frac{\upsilon\Omega(1-\chi)(\sigma_r'-\sigma_\theta')}{\upsilon(1-\chi)^2-\upsilon_0}\right]\right\} \tag{59}$$

The preceding equations can be solved by the corresponding boundary conditions, which are discussed in the next section.

On the other hand, in order to express the results in terms of the position, r, instead of the auxiliary variable, χ, it is necessary to build a connection between r and χ. Differentiating Eq. (45) with respect to r gives

$$\frac{du}{dr} = \chi + r\frac{d\chi}{dr} \tag{60}$$

Combining Eqs. (55) and (60) yields

$$\frac{dr}{r} = \frac{\upsilon(\chi)(1-\chi)}{\upsilon(\chi)(1-\chi)^2-\upsilon_0}d\chi \tag{61}$$

The connection can be obtained by integrating Eq. (61)

$$\frac{r}{a} = \exp\left[\int_{\chi(a)}^{\chi}\frac{\upsilon(\chi)(1-\chi)}{\upsilon(\chi)(1-\chi)^2-\upsilon_0}d\chi\right] \tag{62}$$

Boundary Conditions

The stress components at the elastic-plastic boundary can be expressed as (Li et al. 2016a)

$$\sigma_r'(\chi_p) = \sigma_{h0}' + \frac{p_0'\eta_p^*}{\sqrt{3}} \tag{63}$$

$$\sigma_\theta'(\chi_p) = \sigma_{h0}' - \frac{p_0'\eta_p^*}{\sqrt{3}} \tag{64}$$

$$\sigma_z'(\chi_p) = \frac{3}{1+2K_0}p_0' \tag{65}$$

where χ_p = auxiliary variable at the elastic-plastic boundary; and the relative stress ratio at the elastic-plastic boundary, η_p^*, is

$$\eta_p^*(\chi_p) = M^*\sqrt{\mathrm{OCR}-1} \tag{66}$$

where OCR = overconsolidation ratio.

The value of χ_p can be determined in accordance with Eq. (5)

$$\chi_p = \left(\frac{u}{r}\right)_{r=r_y} = \frac{\sigma_y'(\chi_p)-\sigma_h'}{2G_0} \tag{67}$$

The specific volume at the elastic-plastic boundary is consistent with the value in the elastic zone, and it follows that

$$\upsilon(\chi_p) = \upsilon_0 \tag{68}$$

Making use of the above boundary conditions, the distributions of the stress components and the specific volume around the cavity under the drained condition can be finally determined by solving the differential Eqs. (56)–(59).

Comparisons and Discussion

In order to verify the proposed solutions for the drained cylindrical cavity expansion in natural soils, the results were compared with the published data obtained based on the MCC model (Chen and Abousleiman 2013). The soil adopted in this example was Boston blue clay. It is well known that most naturally deposited soils are found in different consolidation states. Soils with different OCRs usually show different mechanical behaviors. Hence it is quite necessary and meaningful to explore the effects of different OCRs on the drained cylindrical cavity expansion. Here, four different values of OCR were taken, i.e., OCR = 1, 1.2, 3, and 10. Table 1 lists the initial shear modulus, G_0, the initial specific volume, υ_0, and the values of parameters used in the K_0-AMCC model.

For normally consolidated soil (OCR = 1), there is no elastic zone around the cavity. The ratio of the radius of plastic zone to the radius of cylindrical cavity will continuously increase during expansion of the cylindrical cavity. Hence the curve of the elastic-plastic radius with normalized cavity radius for normally consolidated soil does not exist. Fig. 2 shows that the increase in OCR led to a decrease in the elastic-plastic radius, and the magnitude of the decrease was very obvious for slightly or moderately overconsolidated soils (1 < OCR < 3). The present solution differs from the solution proposed by Chen and Abousleiman (2013) when K_0 is less than 1 or greater than 1. The difference of the slightly overconsolidated soil (e.g., OCR = 1.2) was much smaller than that of the heavily overconsolidated soil (e.g., OCR = 10), indicating that

Table 1. Parameters for Boston Blue Clay (Data from Chen and Abousleiman 2013)

K_0	OCR	υ_0	G_0 (kPa)	σ_{h0}' (kPa)	σ_{z0}' (kPa)
0.625	1	2.09	4,348	100	160
0.625	1.2	2.06	4,302	100	160
1.0	3	1.97	4,113	120	120
2.0	10	1.80	3,756	144	72

Note: $M = 1.2$; $\lambda = 0.15$; $\kappa = 0.03$; $v = 0.278$.

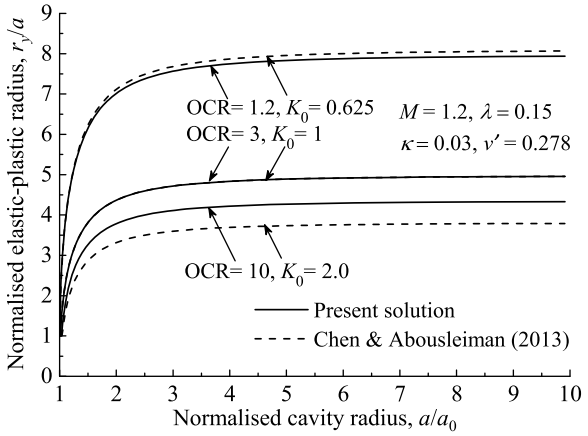

Fig. 2. Comparison of the normalized elastic-plastic radius obtained by the present solution and the published solution

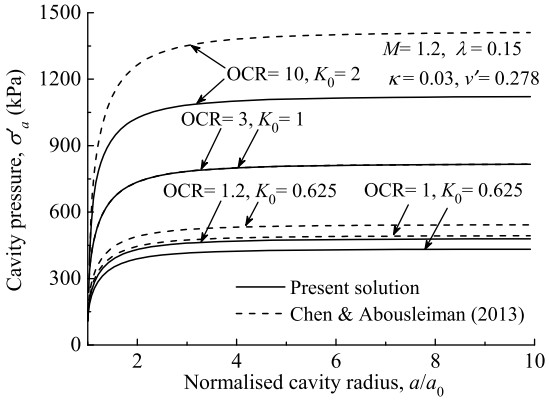

Fig. 3. Comparison of the cavity pressure obtained by the present solution and the published solution

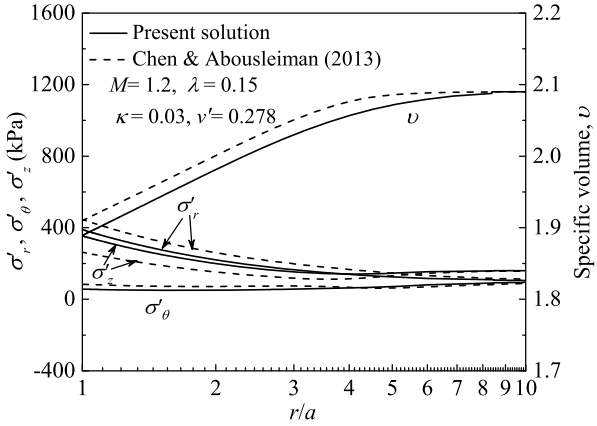

Fig. 4. Comparison of distributions of three stress components and the specific volume surrounding the cavity for normally consolidated soil, OCR = 1 and $K_0 = 0.625$

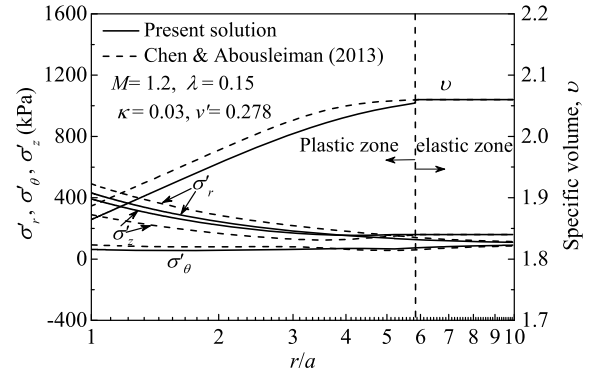

Fig. 5. Comparison of distributions of three stress components and the specific volume surrounding the cavity for slightly overconsolidated soil, OCR = 1.2 and $K_0 = 0.625$

the difference increases with an increase of K_0 when $K_0 > 1$. It also illustrates that the anisotropy of soil plays a significant role in the magnitude of the elastic-plastic radius. The present solutions completely agree with the published solutions when $K_0 = 1$, which indicates that the drained cylindrical cavity expansion based on the K_0-AMCC model reduces to the MCC model-based solutions. Moreover, the elastic-plastic radii with different OCRs increase significantly with smaller normalized cavity radius. However, when the normalized cavity radius is on the order of 7, the elastic-plastic radii nearly remain constant and approach their limit values.

Fig. 3 shows the variation curve of the cavity pressure, σ'_a, plotted against the normalized cavity radius a/a_0. The larger the OCR, the larger is the cavity pressure corresponding to the same normalized cavity radius. The anisotropic effect also plays a pivotal role in the cavity pressure. When K_0 equals 1, the solution reduces to the solution of Chen and Abousleiman (2013).

Figs. 4–7 show the distributions of three stress components and the specific volume around the cylindrical cavity for the soils with different OCRs when the normalized cavity radius a/a_0 is equal to 2. The tangential stress, σ'_θ, varied within a smaller range than the other two stress components (i.e., the radial stress σ'_r and the vertical stress σ'_z). However, an increase of OCR led to relatively strong variations of σ'_θ. At the cavity wall, σ'_r and σ'_z changed significantly and decreased with an increase of the distance from the cavity wall. When r/a became larger, the soil element entered the elastic zone (except OCR = 1), in which the vertical stress remains constant. For normally consolidated soil (OCR = 1) the absolute elastic zone does not exist, although the vertical stress begins to show a smooth trend when r/a is large enough ($r/a > 8$). For the specific volume, υ, it shows a decreasing trend from the elastic zone to the cavity wall. Moreover, larger OCR indicates smaller plastic zone (Figs. 5–7). Compared with the results of Chen and Abousleiman (2013), the proposed solution underestimates σ'_r and υ and overestimates σ'_z in the case of $K_0 < 1$. When $K_0 > 1$, the proposed solution underestimates both σ'_r and σ'_z. The present solutions are consistent with the solution proposed by Chen and Abousleiman (2013) in the case of $K_0 = 1$, indicating that the solution proposed by Chen and Abousleiman (2013) is just a special case (i.e., $K_0 = 1$) of the proposed solution (Fig. 6).

Figs. 8–11 show the distributions of mean effective and deviatoric stresses with specific volume for soils with different OCRs. Points A, B, C represent the in situ stress point, the yield stress point, and the failure stress point, respectively. For normally consolidated soil (OCR = 1), both the mean effective and deviatoric stresses increase with the decrease of the specific volume until they reach the limit values at Point C. For slightly or moderately overconsolidated soils (e.g., OCR = 1.2 and 3), the mean effective stress remains constant (A coincides with B) whereas the deviatoric stress increases when the soil is in the elastic state. After the soil yields, both stresses increase until they reach the limit values. For heavily overconsolidated soil (e.g., OCR = 10), the mean effective

J. Eng. Mech., 2017, 143(11): 04017133

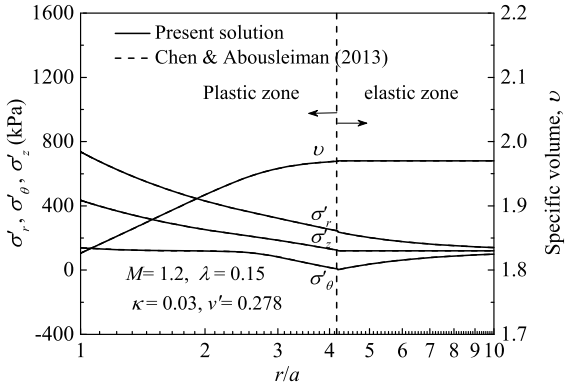

Fig. 6. Comparison of distributions of three stress components and the specific volume surrounding the cavity for moderately overconsolidated soil, OCR = 3 and $K_0 = 1$

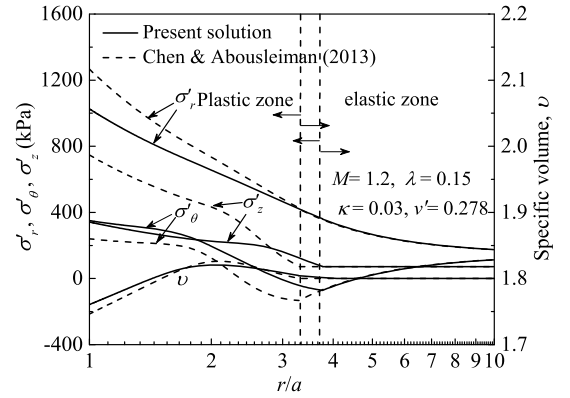

Fig. 7. Comparison of distributions of three stress components and the specific volume surrounding the cavity for heavily overconsolidated soil, OCR = 10 and $K_0 = 2$

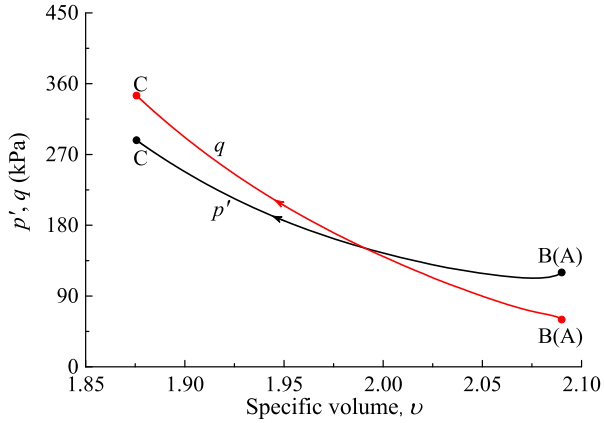

Fig. 8. Distributions of mean effective and deviatoric stresses with specific volume for normally consolidated soil, OCR = 1 and $K_0 = 0.625$

and deviatoric stresses first increase with the increase of the specific volume after the yield of the soil, then they increase with the decrease of the specific volume until they reach the limit values. Different phenomena are found in the variations of mean effective and deviatoric stresses with specific volume for different soils. The reasons for the phenomena are explained in the following section.

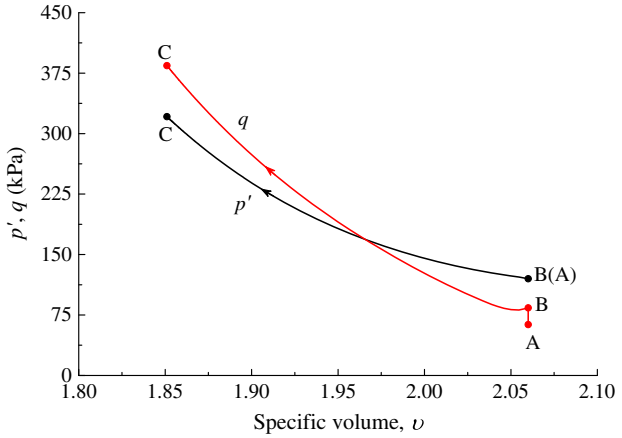

Fig. 9. Distributions of mean effective and deviatoric stresses with specific volume for slightly overconsolidated soil, OCR = 1.2 and $K_0 = 0.625$

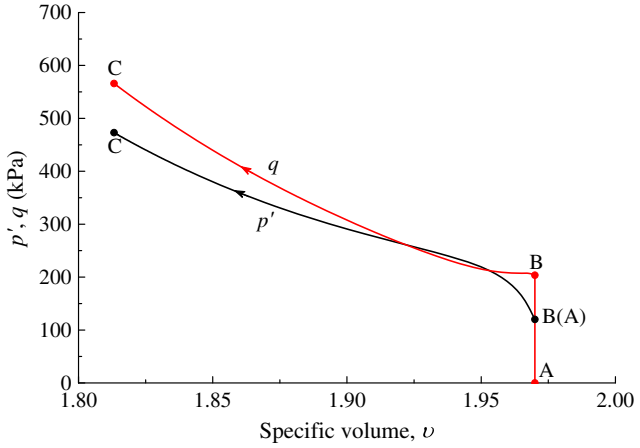

Fig. 10. Distributions of mean effective and deviatoric stresses with specific volume for moderately overconsolidated soil, OCR = 3 and $K_0 = 1$

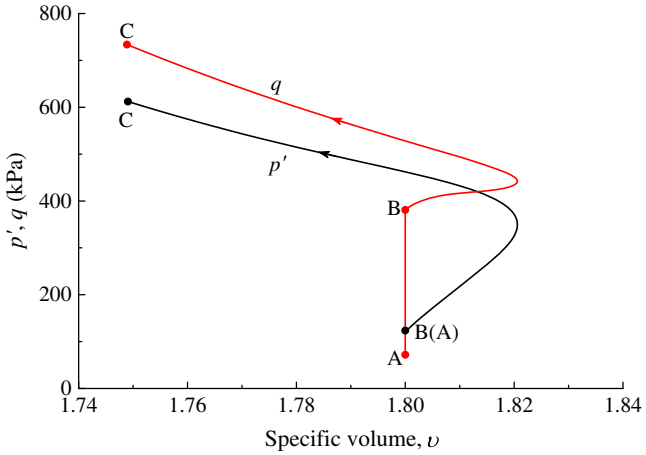

Fig. 11. Distributions of mean effective and deviatoric stresses with specific volume for heavily overconsolidated soil, OCR = 10 and $K_0 = 2$

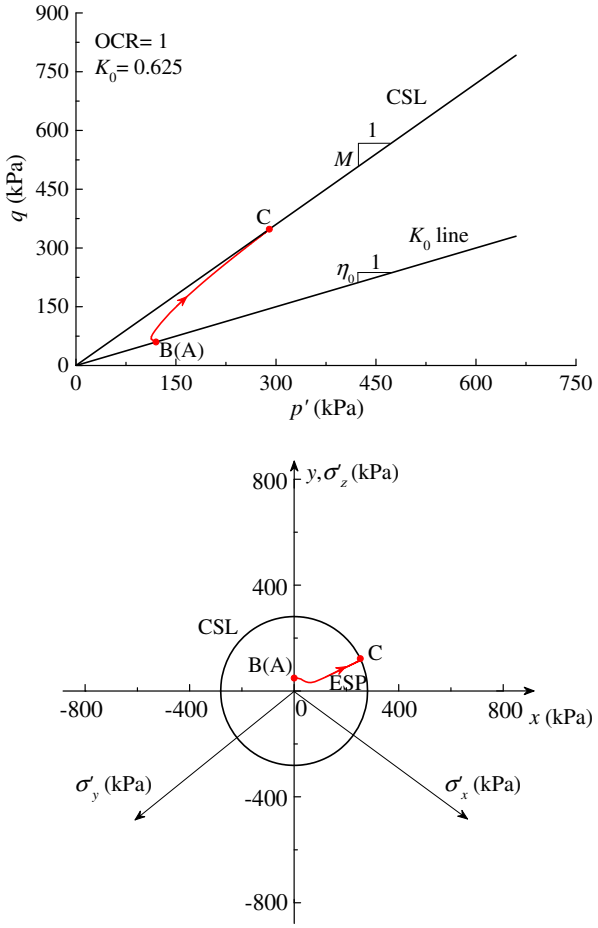

Fig. 12. Stress paths in the $p'-q$ and π planes for normally consolidated soil, OCR = 1, $K_0 = 0.625$

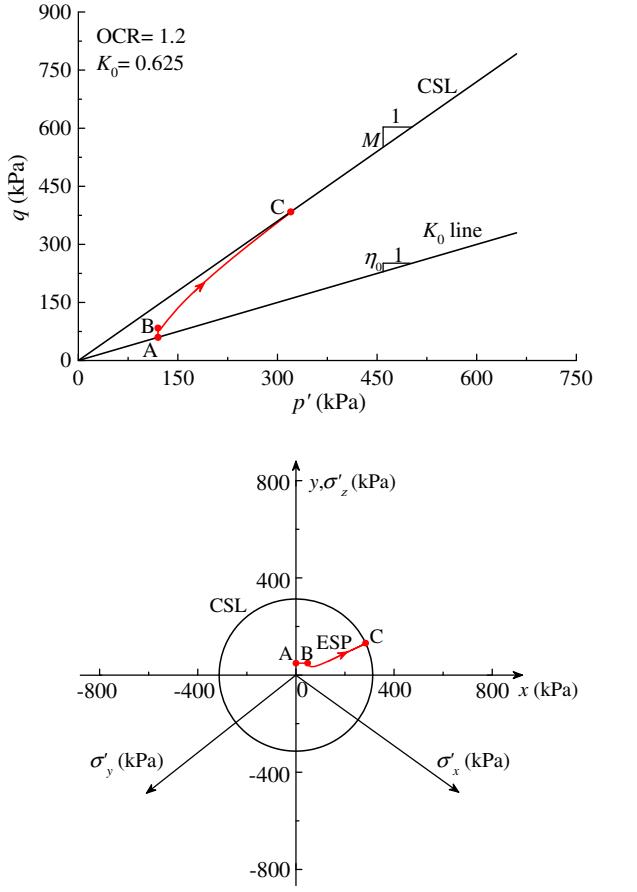

Fig. 13. Stress paths in the $p'-q$ and π planes for slightly overconsolidated soil, OCR = 1.2, $K_0 = 0.625$

Effective Stress Path

The effective stress path can effectively illustrate the change of effective stress of a soil element during the cylindrical cavity expansion. In order to exhibit the three-dimensional property of the ESPs, the $p'-q$ plane and the deviator plane (π plane) are combined to plot the ESPs. The mean stress and the deviator stress follow the standard three-dimensional definitions.

Figs. 12–15 show the ESPs for a soil element at a distance of $4a_0$ from the cavity center at different OCRs. Points A, B, C are as defined in the previous section. This discussion focuses on the ESPs in the $p'-q$ plane. The slope of K_0 line displays the degree of the initial anisotropy. Hence the K_0 line overlaps the p' axis when $K_0 = 1$. For normally consolidated soil (Fig. 12), the stress point first moves to the left, then moves right and upward until it reaches the critical state at Point C. The stress path illustrates that the normally consolidated soil experiences plastic hardening. For slightly or moderately overconsolidated soil (e.g., OCR = 1.2 and 3), the stress point first moves up to the yield stress point B, then moves right until it hits the critical line (CSL) and stays stationary at Point C. As the stress point moves right, the deviator stress first decreases or stays constant, and then increases. Hence the slightly or moderately overconsolidated soil shows a plastic-softening then plastic-hardening behavior. However, the deviator stress of heavily overconsolidated soil increases during the whole process of the cavity expansion, and thus exhibits a plastic-hardening behavior. The ESPs for moderately and heavily overconsolidated soils pass though the critical line (Figs. 14 and 15). This is because the stress increment is tangential to the current yield locus and along the neutral loading direction (Chen and Abousleiman 2013).

Correspondingly, the ESPs for slightly or moderately overconsolidated soils (e.g., OCR = 1.2 and 3) in the π plane first move horizontally toward the right side, and after a decline move upward until they reach the critical line. However, the ESP for heavily overconsolidated soil (e.g., OCR = 10) in the π plane moves horizontally toward the yield stress point B, and then progressively moves downward until it terminates at the failure point C. Fig. 14 shows that for isotropic soil ($K_0 = 1$), before the stress point reaches the yield stress point the coordinate y is equal to 0.

Conclusions

This paper presents a semianalytical solution for the drained cylindrical cavity expansion in natural soils. The K_0-AMCC model, which can incorporate the initial stress anisotropy and the initial stress-induced anisotropy of natural soils, was adopted to model the soil behavior during the cylindrical cavity expansion. The present solution was compared with the existing solution based on the MCC model to investigate the effects of the initial stress anisotropy and the initial stress-induced anisotropy on the cavity expansion, the stress components, and the specific volume by adopting parametric studies with different OCRs. The effective stress paths were also plotted in the $p'-q$ plane and the deviator plane, respectively. The results obtained by this study are briefly summarized as follows:

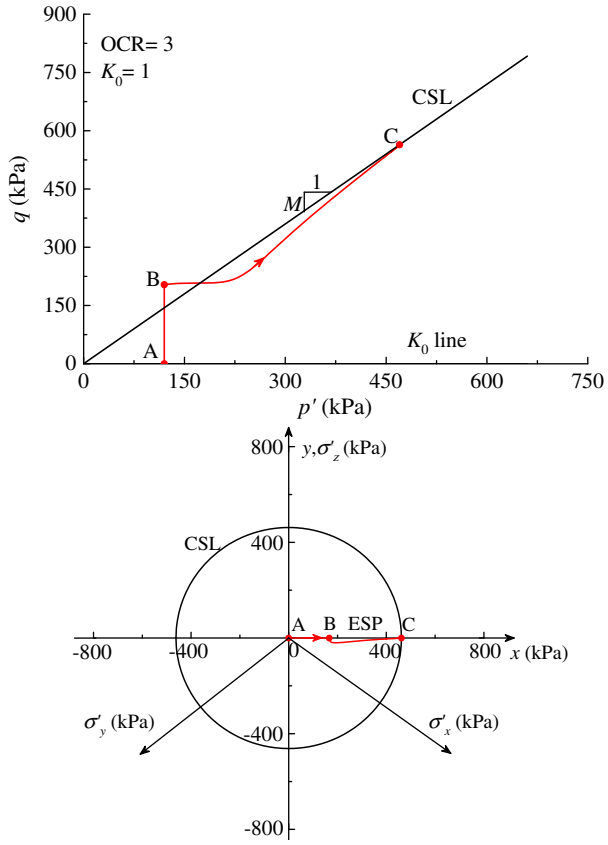

Fig. 14. Stress paths in the $p'-q$ and π planes for moderately overconsolidated soil, OCR = 3, $K_0 = 1$

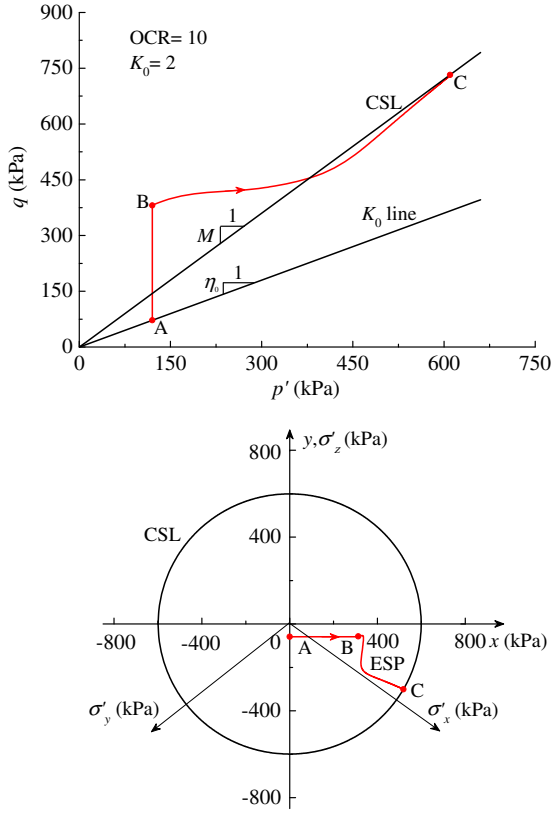

Fig. 15. Stress paths in the $p'-q$ and π planes for heavily overconsolidated soil, OCR = 10, $K_0 = 2$

1. The OCR significantly affects the magnitude of the elastic-plastic radius and the cavity pressure. The increase of OCR leads to an increase of the elastic-plastic radius and a decrease of the cavity pressure. When $K_0 > 1$, the larger coefficient of earth pressure at rest results in the larger difference of the elastic-plastic radius and the cavity pressure between the proposed solution and the solution for isotropic soil.
2. The initial stress anisotropy and the initial stress-induced anisotropy of soils have significant effects on the distributions of the stress components and the specific volume. The proposed solution reduces to the isotropic solution based on the MCC model when $K_0 = 1$.
3. The effective stress paths illustrate that normally consolidated and heavily overconsolidated soils experience plastic hardening during the cylindrical cavity expansion, whereas the slightly and moderately overconsolidated soils display plastic-softening and then plastic-hardening behavior during cylindrical cavity expansion.

Acknowledgments

This research work was supported by the National Natural Science Foundation of China (with Grant Nos. 41272288 and 41572267). The anonymous reviewers' comments have improved the quality of this paper and are also greatly appreciated.

References

Cao, L. F., Teh, C. I., and Chang, M. F. (2001). "Undrained cavity expansion in modified Cam clay." *Géotechnique*, 51(4), 323–334.

Carter, J. P., Booker, J. R., and Yeung, S. K. (1986). "Cavity expansion in cohesive frictional soils." *Géotechnique*, 36(3), 349–358.

Carter, J. P., Randolph, M. F., and Wroth, C. P. (1979). "Stress and pore pressure changes in clay during and after the expansion of a cylindrical cavity." *Int. J. Numer. Anal. Methods Geomech.*, 3(4), 305–322.

Chang, M. F., Teh, C. I., and Cao, L. F. (2001). "Undrained cavity expansion in modified Cam clay. II: Application to the interpretation of the piezocone test." *Géotechnique*, 51(4), 335–350.

Chen, S. L., and Abousleiman, Y. N. (2012). "Exact undrained elastoplastic solution for cylindrical cavity expansion in modified Cam clay soil." *Géotechnique*, 62(5), 447–456.

Chen, S. L., and Abousleiman, Y. N. (2013). "Exact drained solution for cylindrical cavity expansion in modified Cam clay soil." *Géotechnique*, 63(6), 510–517.

Collins, I. F., and Stimpson, J. R. (1994). "Similarity solutions for drained and undrained cavity expansions in soils." *Géotechnique*, 44(1), 21–34.

Collins, I. F., and Yu, H. S. (1996). "Undrained cavity expansions in critical state soils." *Int. J. Numer. Anal. Methods Geomech.*, 20(7), 489–516.

Falagush, O., McDowell, G. R., Yu, H. S., and de Bono, J. P. (2015). "Discrete element modelling and cavity expansion analysis of cone penetration testing." *Granular Matter*, 17(4), 483–495.

Frikha, W., and Bouassida, M. (2013). "Cylindrical cavity expansion in elastoplastic medium with a variable potential flow." *Int. J. Geomech.*, 10.1061/(ASCE)GM.1943-5622.0000166, 9–15.

Guo, W. D. (2000). "Visco-elastic consolidation subsequent to pile installation." *Comput. Geotech.*, 26(2), 113–144.

Hill, R. (1950). *The mathematical theory of plasticity*, Oxford University Press, London.

Lamé, G. (1852). *Leçons sur la théorie mathématiques de l'élasticité des corps solides*, Bachelier, Paris (in French).

Li, L., Li, J., and Sun, D. A. (2016a). "Anisotropically elasto-plastic solution to undrained cylindrical cavity expansion in K_0-consolidated clay." *Comput. Geotech.*, 73, 83–90.

Li, L., Li, J., Sun, D. A., and Gong, W. (2017). "Analysis of time-dependent bearing capacity of a driven pile in clayey soils by total stress method." *Inter. J. Geomech.*, 10.1061/(ASCE)GM.1943-5622.0000860, 04016156.

Li, J., Li, L., Sun, D. A., and Rao, P. (2016b). "Analysis of undrained cylindrical cavity expansion considering three-dimensional strength of soils." *Int. J. Geomech.*, 10.1061/(ASCE)GM.1943-5622.0000650, 04016017.

Mabsout, M. E., Sadek, S. M., and Smayra, T. E. (1999). "Pile driving by numerical cavity expansion." *Int. J. Numer. Anal. Methods Geomech.*, 23(11), 1121–1140.

Marshall, A. M. (2012). "Tunnel-pile interaction analysis using cavity expansion methods." *J. Geotech. Geoenviron. Eng.*, 10.1061/(ASCE)GT.1943-5606.0000709, 1237–1246.

Matsuoka, H., and Sun, D. A. (2006). *The SMP concept-based 3D constitutive models for geomaterials*, Taylor & Francis, London.

Mo, P. Q., Marshall, A. M., and Yu, H. S. (2017). "Interpretation of cone penetration test data in layered soils using cavity expansion analysis." *J. Geotech. Geoenviron. Eng.*, 10.1061/(ASCE)GT.1943-5606.0001577, 04016084.

Mo, P. Q., and Yu, H. S. (2017). "Undrained cavity expansion analysis with a unified state parameter model for clay and sand." *Géotechnique*, 67(6), 503–515.

Randolph, M. F. (2003). "Science and empiricism in pile foundation design." *Géotechnique*, 53(10), 847–875.

Randolph, M. F., Carter, J. P., and Wroth, C. P. (1979). "Driven piles in clay-the effects of installation and subsequent consolidation." *Géotechnique*, 29(4), 361–393.

Roscoe, K. H., Schofield, A., and Thurairajah, A. (1963). "Yielding of clays in states wetter than critical." *Géotechnique*, 13(3), 211–240.

Schofield, A., and Wroth, P. (1968). *Critical state soil mechanics*, McGraw-Hill, New York.

Vesic, A. S. (1972). "Expansion of cavities in infinite soil mass." *J. Soil Mech. Found. Div.*, 98(SM3), 265–290.

Vrakas, A., and Anagnostou, G. (2015). "Finite strain elastoplastic solutions for the undrained ground response curve in tunnelling." *Int. J. Numer. Anal. Methods Geomech.*, 39(7), 738–761.

Wood, D. M. (1990). *Soil behaviour and critical state soil mechanics*, Cambridge University Press, Cambridge, U.K.

Yao, Y. P., Hou, W., and Zhou, A. N. (2009). "UH model: Three-dimensional unified hardening model for overconsolidated clays." *Géotechnique*, 59(5), 451–469.

Yu, H. S. (2000). *Cavity expansion methods in geomechanics*, Kluwer Academic Publishers, Dordrecht, Netherlands.

Yu, H. S., and Rowe, R. K. (1999). "Plasticity solutions for soil behaviour around contracting cavities and tunnels." *Int. J. Numer. Anal. Methods Geomech.*, 23(12), 1245–1279.

Yu, H. S., Schnaid, F., and Collins, I. F. (1996). "Analysis of cone pressuremeter tests in sands." *J. Geotech. Eng.*, 10.1061/(ASCE)0733-9410(1996)122:8(623), 623–632.

Zhou, H., Kong, G., and Liu, H. (2016). "A semi-analytical solution for cylindrical cavity expansion in elastic-perfectly plastic soil under biaxial in situ stress field." *Géotechnique*, 66(7), 584–595.

Zhou, H., Liu, H., Kong, G., and Huang, X. (2014). "Analytical solution of undrained cylindrical cavity expansion in saturated soil under anisotropic initial stress." *Comput. Geotech.*, 55, 232–239.